

Color-Pure Violet-Light-Emitting Diodes Based on Layered Lead Halide Perovskite Nanoplates

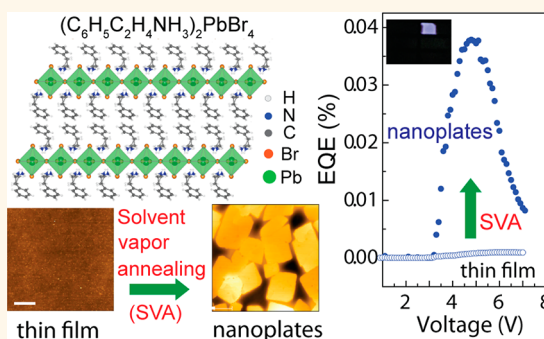
Dong Liang,^{†,§} Yuelin Peng,^{‡,§} Yongping Fu,[†] Melinda J. Shearer,[†] Jingjing Zhang,[†] Jianyuan Zhai,[†] Yi Zhang,[†] Robert J. Hamers,[†] Trisha L. Andrew,^{*,†} and Song Jin^{*,†}

[†]Department of Chemistry and [‡]Department of Electrical and Computer Engineering, University of Wisconsin–Madison, Madison, Wisconsin 53706, United States

S Supporting Information

ABSTRACT: Violet electroluminescence is rare in both inorganic and organic light-emitting diodes (LEDs). Low-cost and room-temperature solution-processed lead halide perovskites with high-efficiency and color-tunable photoluminescence are promising for LEDs. Here, we report room-temperature color-pure violet LEDs based on a two-dimensional lead halide perovskite material, namely, 2-phenylethylammonium ($C_6H_5CH_2CH_2NH_3^+$, PEA) lead bromide $[(PEA)_2PbBr_4]$. The natural quantum confinement of two-dimensional layered perovskite $(PEA)_2PbBr_4$ allows for photoluminescence of shorter wavelength (410 nm) than its three-dimensional counterpart. By converting as-deposited polycrystalline thin films to micrometer-sized $(PEA)_2PbBr_4$ nanoplates using solvent vapor annealing, we successfully integrated this layered perovskite material into LEDs and achieved efficient room-temperature violet electroluminescence at 410 nm with a narrow bandwidth. This conversion to nanoplates significantly enhanced the crystallinity and photophysical properties of the $(PEA)_2PbBr_4$ samples and the external quantum efficiency of the violet LED. The solvent vapor annealing method reported herein can be generally applied to other perovskite materials to increase their grain size and, ultimately, improve the performance of optoelectronic devices based on perovskite materials.

KEYWORDS: layered perovskite, violet-light-emitting diode (LED), solvent vapor annealing, nanoplate



Organic and direct-band-gap inorganic semiconductors have been studied and employed for energy-efficient optoelectronic devices for display and lighting applications in the past few decades.^{1,2} Despite these efforts, violet-colored (<450 nm) light-emitting diodes (LEDs) are quite rare³ and expensive to make, but very desirable for a variety of applications. Violet LEDs are key optoelectronic components that can enable wide-gamut, full-color displays,⁴ fluorescence-based chemical and biological sensors,⁵ and optical detectors.⁶ Currently, violet LEDs are made of InGaN, but they are fabricated *via* expensive high-temperature and high-vacuum thin-film growth techniques.⁷ Therefore, it is important to find inexpensive and easily processed materials as the emitters in blue or violet LEDs.

Recently, organic–inorganic hybrid perovskites, particularly the three-dimensional (3D) perovskites represented by methylammonium (MA) lead iodide,^{8–11} have emerged as an excellent class of semiconductors with long charge carrier lifetime and diffusion lengths^{12–14} and high photoluminescence (PL) quantum yield.¹⁵ These excellent properties not only enable high-performance solar cells^{8–11} with high internal quantum efficiency¹⁶ but also make these perovskite materials promising for LED, lasing, and photodetector applications.^{17–22} In addition, films of metal halide perovskites can be accessed

via simple solution processing at room temperature, and their photoluminescence can be easily tuned from the visible to infrared wavelengths.^{15,23} Efficient lasing in 3D organometal halide perovskites has been previously demonstrated,^{15,18,23,24} and various LEDs containing 3D MA lead halide perovskites^{17,18,25,26} and cesium lead halide perovskites^{27,28} as the luminescent component have also been reported. Although optimized MA perovskite LEDs have recently reached an external quantum efficiency (EQE) over 8% for green light emission,¹⁸ efficient blue electroluminescence has not been achieved yet due to the high defect densities typically associated with wider-band-gap lead chloride perovskites.^{15,23,24,29,30} A cesium lead halide perovskite quantum dot LED with an emitting peak of 455 nm and EQE of 0.07% has been reported very recently.²⁷ Clearly, it has been difficult to extend the efficient electroluminescence (EL) of 3D perovskite-containing LEDs to blue wavelengths, and no violet perovskite LEDs have been reported yet.

Received: April 21, 2016

Accepted: June 23, 2016

Published: June 23, 2016

Transitioning from 3D lead halide perovskites into two-dimensional (2D) structures^{31–33} will introduce quantum confinement effects in these materials, and, therefore, 2D lead halide perovskites are expected to display wider band gaps and narrower photoluminescence peaks as compared to their 3D analogues.^{34,35} Following this logic, one potential strategy to obtain violet PL is to synthesize 2D versions of green-emitting 3D lead bromide perovskites. Layered 2D organolead halide perovskites are described by the general formula $(\text{RNH}_3)_2\text{PbX}_4$, where R is an aryl or alkyl substituent and X is a halogen.^{31–33} Specifically, using 2-phenylethylammonium ($\text{C}_6\text{H}_5\text{CH}_2\text{CH}_2\text{NH}_3^+$, PEA, also called phenethylammonium) as the organic cation yields 2D layered perovskites $(\text{PEA})_2\text{PbBr}_4$ (crystal structure shown in Figure 1A),³⁶ in

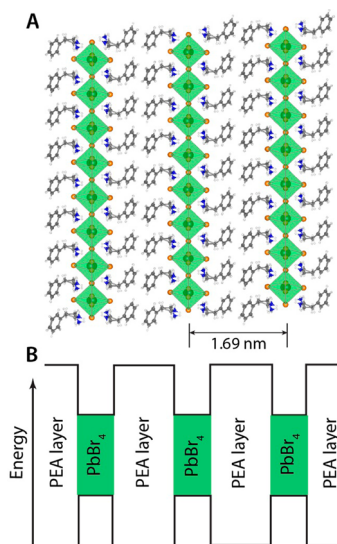


Figure 1. (A) Crystal structure of 2-phenylethylammonium lead bromide, $(\text{PEA})_2\text{PbBr}_4$, which is a 2D layered perovskite. The inorganic layers consist of corner-sharing lead bromide octahedra in which the green and orange balls represent Pb and Br atoms, respectively. The organic layers consist of PEA cations. The gray balls represent carbon atoms, the white balls represent hydrogen atoms, and the blue balls represent nitrogen atoms. (B) Schematic energy diagram showing multiple quantum wells in layered $(\text{PEA})_2\text{PbBr}_4$.

which layers of the inorganic semiconductor (sheets of corner-sharing PbBr_6 octahedra) are sandwiched between layers of insulating PEA counter cations. The spacing between inorganic layers is 1.69 nm. Electronic coupling between inorganic layers is negligible because of the high energy barriers formed by the PEA layers. This 2D material naturally forms repeating quantum well structures, as schematically shown in Figure 1B, that tightly confine excitons within the inorganic layers, leading to high exciton binding energies (350–480 meV)³⁷ and strong, stable PL at room temperature.³⁶ Narrow, violet PL was previously reported for $(\text{PEA})_2\text{PbBr}_4$.³⁸ The quantum confinement and high exciton binding energies are believed to increase the LED efficiency.³⁹ However, to date, such 2D perovskites have not been successfully integrated as the light-emitting material into LEDs that can be operated at room temperature. Green LEDs incorporating 2D PEA lead iodide [$(\text{PEA})_2\text{PbI}_4$] were previously reported to function exclusively at liquid nitrogen temperatures,⁴⁰ thus precluding their practical applications. We note that there was also an earlier report on

green LED devices based on a 2D layered perovskite; however, in those devices, light emission came from the dye molecules incorporated in the 2D layered perovskite and the perovskite framework merely served as a template but not the active light-emitting materials.⁴¹

Here, we demonstrate a color-pure, room-temperature-operable violet LED containing a 2D layered perovskite, 2-phenylethylammonium lead bromide, $(\text{PEA})_2\text{PbBr}_4$, as the luminescent layer. The LED displayed a narrow electroluminescence peak centered at 410 nm, with a full width at half-maximum (fwhm) of 14 nm. Critical to this success of room-temperature LEDs based on 2D layered perovskites as active materials with a reasonable efficiency is a solvent vapor annealing technique that converted as-deposited polycrystalline $(\text{PEA})_2\text{PbBr}_4$ thin films into high-quality micrometer-sized nanoplates, which was found to enhance both the photo-physical properties of this 2D perovskite and the external quantum efficiency of the LEDs fabricated with this material.

RESULTS AND DISCUSSION

The chemical synthesis of $(\text{PEA})_2\text{PbBr}_4$ can be readily accomplished by mixing PEABr and PbBr_2 precursors at room temperature.³⁶ But the key for LED device fabrication is the preparation of suitable thin-film samples in relevant device architecture. The various $(\text{PEA})_2\text{PbBr}_4$ perovskite samples used in this study were accessed *via* a common precursor thin film that was obtained by spin-coating a dimethylformamide (DMF) solution of PEABr and PbBr_2 (in a 2:1 molar ratio) onto poly(3,4-ethylenedioxythiophene):poly(styrenesulfonate) (PEDOT:PSS)-coated ITO substrates (Figure 2A). Detailed

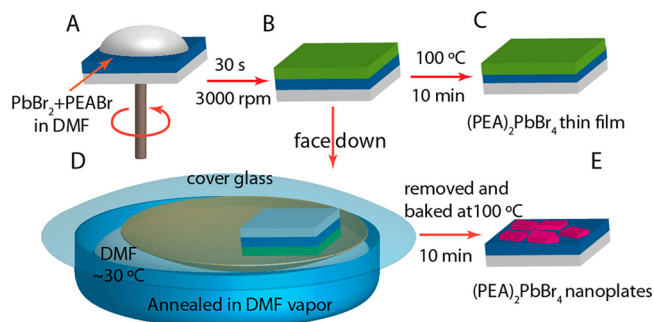


Figure 2. Synthesis of $(\text{PEA})_2\text{PbBr}_4$ thin films and nanoplates on PEDOT:PSS-coated ITO substrates. (A, B) A DMF solution of 2:1 PEA bromide (PEABr) and PbBr_2 is spin-coated onto a PEDOT:PSS (blue) coated ITO substrate (gray). The spin-coated film was either directly baked at 100 °C for 10 min to prepare polycrystalline $(\text{PEA})_2\text{PbBr}_4$ thin films (C) or annealed in DMF vapor (D) and then baked at 100 °C for 10 min to prepare (E) micrometer-sized $(\text{PEA})_2\text{PbBr}_4$ nanoplates (purple).

experimental procedures are provided in the Methods section. Here we take advantage of the fact that the PEDOT:PSS film is hydrophilic, which facilitates the coating of this precursor film with good coverage. The precursor films thus obtained looked green to the naked eye (Figure 2B).

Two types of $(\text{PEA})_2\text{PbBr}_4$ samples were then prepared from these precursor thin films. For the first type, a polycrystalline $(\text{PEA})_2\text{PbBr}_4$ sample was accessed by directly baking the precursor film at 100 °C for 10 min on a hot plate in air, shown in Figure 2C. The second type was micrometer-sized nanoplates of $(\text{PEA})_2\text{PbBr}_4$, which were accessed by first annealing the precursor film face-down in a cover glass covered

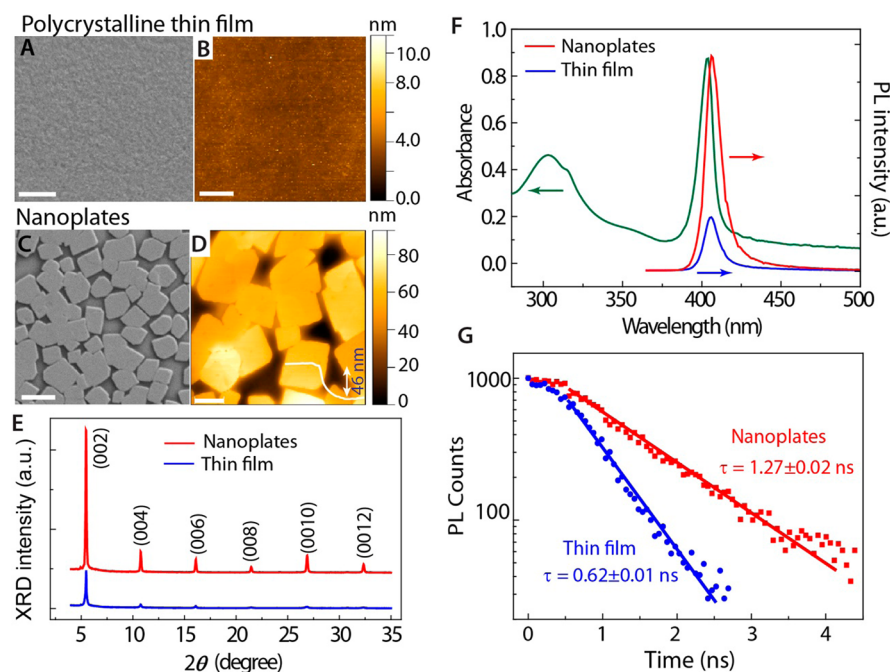


Figure 3. (A) SEM and (B) AFM images of the $(\text{PEA})_2\text{PbBr}_4$ thin film without DMF treatment. The scale bars are both $2\ \mu\text{m}$. (C) SEM and (D) AFM images of the $(\text{PEA})_2\text{PbBr}_4$ nanoplates obtained by annealing the thin film in DMF vapor before baking. The scale bars in panels C and D are 2 and $1\ \mu\text{m}$, respectively. The inset white profile curve of D shows a nanoplate thickness of 46 nm. (E) XRD patterns of polycrystalline thin film (blue) and nanoplates (red). (F) Absorbance spectrum (green) and photoluminescence of the thin film (blue) and nanoplates (red). (G) PL photon counts as a function of time for polycrystalline thin film (blue) and nanoplates (red) excited by a 370 nm light pulse. The lines are linear fits. XRD patterns and PL and PL lifetimes are taken for nanoplates synthesized in the same conditions as the thin film except for the additional DMF vapor annealing.

beaker in DMF vapor at about $30\ ^\circ\text{C}$, before baking at $100\ ^\circ\text{C}$ in air, shown in Figure 2D,E. A detailed description of the DMF solvent annealing procedure and experimental setup is provided in the Methods section. As the DMF was vaporized and absorbed by the spin-coated thin film, it initiated and facilitated the recrystallization of the thin film into many perovskite nanoplates. The precursor films were observed to significantly change color from green to purple upon DMF vapor annealing due to the light scattering caused by the $(\text{PEA})_2\text{PbBr}_4$ nanoplates. This color changing phenomenon was used to time the DMF annealing process across different samples, which usually took 3 to 5 min. The thickness of the layer of $(\text{PEA})_2\text{PbBr}_4$ nanoplates obtained from the DMF vapor annealing procedure was found to depend on the concentration of the starting $\text{PEABr}/\text{PbBr}_2$ solution in DMF and spin-coating speed, as discussed in more detail later.

The $(\text{PEA})_2\text{PbBr}_4$ samples prepared through these two approaches have distinctively different morphology and photo-physical properties. The scanning electron microscopy (SEM) and atomic force microscopy (AFM) images (Figure 3A and B, respectively) revealed that the polycrystalline samples obtained *via* direct baking are smooth and uniform on PEDOT:PSS/ITO substrates. The thickness of these polycrystalline thin films is $\sim 30\ \text{nm}$ with surface roughness about 2 nm. In contrast, the samples obtained upon DMF vapor annealing/baking can be described as a two-dimensional ensemble of micrometer-sized, square-faceted nanoplates (Figure 3C and D). Height profiles obtained from AFM scans indicate that the thickness of the $(\text{PEA})_2\text{PbBr}_4$ nanoplates obtained from a 6.7 wt % DMF solution of $\text{PEABr}/\text{PbBr}_2$ is approximately 46 nm. The nanoplates are distributed evenly on the PEDOT:PSS/ITO substrate, although there are empty spaces between nanoplates.

The X-ray diffraction (XRD) patterns shown in Figure 3E confirmed the phase of both the thin film and nanoplates to be single-phase layered perovskite structures with signature peaks corresponding to the layered structure type, which is consistent with previous reports.³⁴ The dominance of the (00*l*) peaks in the XRD pattern suggests that the crystals of both thin-film and nanoplate samples were highly oriented, with the *c*-axis perpendicular to the substrate plane,³⁸ although the crystal grains of the thin-film sample are too small to be observed under SEM. More importantly, the XRD peak intensity from the DMF vapor-treated sample is much stronger than the thin-film sample, which indicates better crystallinity for the nanoplate sample than the thin film. Enhanced crystallinity in organometal lead halide perovskites has been previously achieved *via* solvent vapor annealing with toluene⁴² and spin-coating onto nonwetting substrates.⁴³ Therefore, it is not surprising that the DMF vapor-annealed nanoplate sample reported herein has larger crystal grains than the polycrystalline thin-film sample as reported before.⁴⁴

The green curve in Figure 3F represents the absorbance spectra of both the perovskite polycrystalline thin film and nanoplate samples, since their absorbance spectra are exactly the same after being normalized to [0,1]. The absorbance spectrum indicates a strong excitonic band centered at 404 nm, consistent with previous reports.^{36,38} Both polycrystalline films and nanoplates display a single photoluminescence peak at 407 nm (Figure 3F) when excited at 370 nm. The PL intensity of the nanoplate sample was observed to be greater than that of the polycrystalline sample (at the same absorbance optical densities), indicating a higher PL quantum yield in the nanoplates. Indeed, the PL quantum yield of the polycrystalline thin-film samples was measured to be 10%, whereas that of the

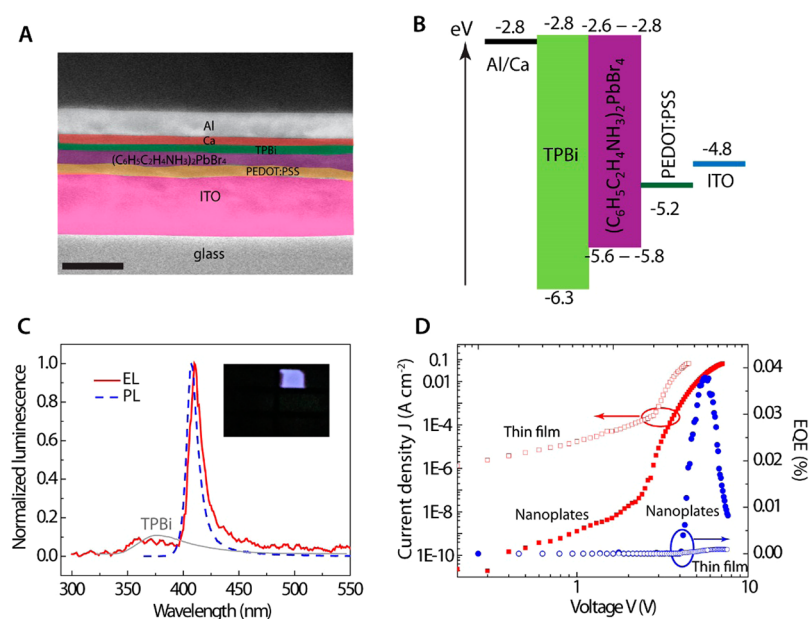


Figure 4. (A) Cross-sectional SEM image of the $(\text{PEA})_2\text{PbBr}_4$ LED devices. The scale bar is 200 nm. (B) Energy-level diagram for the $(\text{PEA})_2\text{PbBr}_4$ LED devices. The valence band edge of $(\text{PEA})_2\text{PbBr}_4$ was measured by UPS, and the conduction band edge calculated from the optical gap; other values were taken from refs 42, 43, and 45. (C) Normalized luminescence of a typical LED device based on $(\text{PEA})_2\text{PbBr}_4$ nanoplates obtained from DMF vapor annealing operated at 6 V. The EL and PL peaks are located at 410 and 407 nm, respectively. The weak EL peak at 375 nm is from TPBi, consistent with its PL (gray curve). The inset shows a picture of uniform violet light emission from a $(\text{PEA})_2\text{PbBr}_4$ LED device. (D) Current–voltage (J – V) dependence (red symbols) and EQEs (blue symbols) for LEDs fabricated with a $(\text{PEA})_2\text{PbBr}_4$ thin film (open symbols) and nanoplates (solid symbols).

nanostructures was measured to be 26%. The PL lifetime of these films was measured using wavelength-resolved, time-correlated single-photon counting with pulsed 370 nm excitation. The excited-state lifetime of nanoplates was found to be 1.27 ± 0.02 ns, approximately 2 times longer than that of polycrystalline thin films (0.62 ± 0.01 ns). Notably, the measured excited-state lifetimes of the various $(\text{PEA})_2\text{PbBr}_4$ layered perovskite films reported herein are slightly lower than bulk single crystals of $(\text{PEA})_2\text{PbBr}_4$ ³⁶ and much lower than those of the 3D MA lead halide perovskites (usually 10's of ns).^{12,13,24} Overall, the $(\text{PEA})_2\text{PbBr}_4$ nanoplate samples with large grain sizes enabled by the DMF solvent vapor annealing exhibited enhanced intensities in XRD and PL, as well as increased PL lifetimes, as compared to polycrystalline thin-film samples. The increase of crystal grain sizes could lower the defect density and, thus, enhance the PL signal in $(\text{PEA})_2\text{PbBr}_4$ nanoplate samples. Improving the crystallinity and increasing the grain size of 3D organometal halide perovskites have been previously shown to enhance their PL quantum yield and photovoltaic and lasing performance,^{14,24,43,45,46} consistent with the observations reported herein for 2D perovskites.

Light-emitting diodes were then fabricated using both $(\text{PEA})_2\text{PbBr}_4$ polycrystalline thin films and nanoplates. Starting from the $(\text{PEA})_2\text{PbBr}_4$ samples deposited on PEDOT:PSS-coated ITO substrates, the diode structure was completed by sequentially depositing an organic electron transport layer (TPBi) and metal top cathode (Ca/Al) *via* physical vapor deposition under ultrahigh vacuum (see detailed fabrication procedures in the [Methods](#) section). The final device structure was ITO/PEDOT:PSS (30 nm)/ $(\text{PEA})_2\text{PbBr}_4$ /TPBi (35 nm)/Ca (25 nm)/Al (100 nm), and the LED device area was 3.6 mm². [Figure 4A](#) presents a cross-sectional SEM image of a typical $(\text{PEA})_2\text{PbBr}_4$ nanoplate LED device. A schematic flat-band energy-level diagram is shown in [Figure 4B](#). In the device

structure, ITO serves as a bottom electrode, PEDOT:PSS (work function -5.2 eV)⁴⁷ works as a hole transport layer, TPBi (LUMO -2.8 eV, HOMO -6.3 eV)⁴⁸ serves as an electron transport layer, Ca (work function -2.8 eV)⁴⁹ is used as an efficient electron injection layer, and Al works as a top electrode. Since the perovskite layer has been baked to fully remove the DMF residue, and a layer of TPBi was deposited between the perovskite and Ca layers, there should be no chemical reaction between the perovskite and the Ca layer. We measured the valence band edges and work functions of the $(\text{PEA})_2\text{PbBr}_4$ samples using ultraviolet photoemission spectroscopy (UPS), as shown in [Figure S1](#) in the [Supporting Information](#). UPS measurements revealed that the work function was 4.86 eV for the polycrystalline thin-film samples and 4.34 eV for the nanoplate samples ([Figure S1C](#)). The valence band edge was measured to be located at 0.99 and 1.27 eV below the Fermi level of polycrystalline thin films and nanoplates, respectively ([Figure S1D](#)), which correspond to -5.85 and -5.61 eV (*vs* the vacuum level). Using the optical band gap of 3.0 eV obtained from the absorbance spectrum in [Figure 3F](#), the conduction band edge is calculated to lie at -2.85 eV (*vs* the vacuum level) for polycrystalline samples and -2.61 eV for nanoplates. The differences of the UPS data between the nanoplates and the thin films are likely caused by the changes in their surface states and morphology, as differences in the number of defects, edges, or grain boundaries in samples can shift UPS spectra.⁵⁰

The electroluminescence spectrum of a typical $(\text{PEA})_2\text{PbBr}_4$ nanoplate LED ([Figure 4C](#), red curve) displayed a major peak centered at 410 nm with an ultranarrow fwhm of 14 nm. The EL spectrum was observed to be red-shifted by 3 nm from the PL emission peak of $(\text{PEA})_2\text{PbBr}_4$, most likely due to minor optical cavity effects. The inset shows a typical photo of a device emitting violet light in the dark. The weak EL peak at

375 nm can be ascribed to electroluminescence from TPBi; a characteristic PL curve for TPBi is provided for reference in Figure 4C (gray curve). Some bleed-through EL from the TPBi layer is expected in the $(\text{PEA})_2\text{PbBr}_4$ nanoplate LEDs reported herein because of discontinuous surface coverage by the nanoplate layer: direct contact between the PEDOT:PSS hole injection layer and the TPBi electron injection layer occurs in the empty spaces between nanoplates, which can lead to exciton formation in the TPBi layer. But the EL from TPBi never dominates the device performance at the operating voltage of these devices.

The current density–voltage curves of both the $(\text{PEA})_2\text{PbBr}_4$ polycrystalline thin film and nanoplate LEDs (Figure 4D) revealed standard diode behavior and turn-on voltages of 2.8 and 2.5 V, respectively. This difference of turn-on voltage is due to the worse charge carrier confinement of the thin-film layer than in the nanoplate layer. The log–log curves clearly revealed that the devices fabricated with $(\text{PEA})_2\text{PbBr}_4$ nanoplates exhibit lower leakage currents at subthreshold voltages than those based on polycrystalline thin films due to the good electron and hole confinement of the quantum structure of the $(\text{PEA})_2\text{PbBr}_4$ nanoplates. Accordingly, the EQE of devices incorporating polycrystalline $(\text{PEA})_2\text{PbBr}_4$ thin films was found to be very low (0.002%) at room temperature. This low EQE value is consistent with the poor room-temperature light output previously reported for other LEDs incorporating 2D layered perovskites.⁴⁰ Significantly, upon converting the polycrystalline $(\text{PEA})_2\text{PbBr}_4$ thin films to single-crystal nanoplates *via* the DMF solvent vapor annealing, the EQE of $(\text{PEA})_2\text{PbBr}_4$ LEDs was increased to 0.04% for the champion device, 20 times higher than that of the polycrystalline thin film $(\text{PEA})_2\text{PbBr}_4$ LEDs. All these results show that DMF vapor annealing is a powerful processing step that greatly enhances the crystallinity of 2D layered perovskites and elevates the functionality and operability of 2D perovskite-based optoelectronic devices.

We note that as the initial demonstration of room-temperature violet EL from a 2D perovskite material, the 0.04% EQE value measured for our $(\text{PEA})_2\text{PbBr}_4$ nanoplate LEDs is a respectable starting point. As a violet-light-emitting material, 2D layered $(\text{PEA})_2\text{PbBr}_4$ perovskite leads to devices with EQEs comparable to those initially fabricated with other nanostructured emitter materials. For example, the initially reported CdS/ZnS core–shell quantum dot LEDs displayed external quantum efficiencies of approximately 0.1% at 459 nm.⁵¹ The initial green-emitting (517 nm) LED based on 3D methylammonium lead bromide perovskite exhibited an EQE of 0.1%.¹⁷ Furthermore, the significant recent progress made in LEDs based on 3D lead halide perovskites^{17,18,25,26} has not been translated into the blue wavelength ranges, and all of the reported LEDs based on chloride-containing perovskites showed much lower efficiency than their longer wavelength counterparts based on bromide or iodide perovskites.^{26,29,30} For example, the recently reported blue-emitting LED based on CsPbX_3 perovskite quantum dots has reached an EQE of only 0.07% at 455 nm.²⁷ In contrast, at an emission wavelength of 410 nm, the $(\text{PEA})_2\text{PbBr}_4$ LED devices reported herein are the first violet LEDs not only based on perovskite materials but also based on 2D perovskites as active materials that can be operated at room temperature.

The dependence of the EQE of nanoplate LED devices on the concentration of the PEABr/PbBr_2 precursor solution used for spin-coating was also studied to reach the optimal device discussed above. As the precursor solution concentration was

changed from 3.4 wt % to 13.4 wt %, the thickness of the nanoplates (as measured by AFM) varied from 30 to 100 nm, as summarized in Table 1. Clearly, high precursor concen-

Table 1. Dependence of the EQE of the LED Devices and the Thickness of the $(\text{PEA})_2\text{PbBr}_4$ Nanoplates on the PEABr/PbBr_2 Precursor Concentration in DMF

PEABr/PbBr ₂ concentration (wt %)	noplate thickness (nm)	EQE (%)
3.4	30	0.008
6.7	50	0.038
10	80	0.024
13.4	100	0.013

trations yielded thicker nanoplates. LEDs of various nanoplate layer thickness were fabricated following the same device fabrication procedures. As shown in Table 1 (and Figure S3 in the Supporting Information), a precursor concentration of 6.7 wt % was found to yield the highest EQE. Informed by scientific advances made in fabricating quantum dot LEDs,⁵² one expects the EQE of the $(\text{PEA})_2\text{PbBr}_4$ perovskite nanoplate LEDs described herein to increase with decreasing perovskite layer thickness. This prediction stems from the fact that a thinner luminescent layer leads to higher electron–hole recombination efficiency, which ultimately results in increased light output. Indeed, higher device EQE was observed with decreasing nanoplate layer thickness, down to about 50 nm. Below a thickness of 50 nm, however, the EQE of nanoplate LEDs was observed to decrease again due to nonuniform nanoplate coverage on the PEDOT:PSS/ITO substrate. As shown in Figure S2 in the Supporting Information, the morphology of $(\text{PEA})_2\text{PbBr}_4$ samples also changed from nanoplate to needle-like nanoribbons if the starting precursor concentration was decreased below approximately 6 wt %. Low sample coverage causes large leaking current and low light-emitting intensity, thus lowering the LED efficiency. The EQE could be further improved if we could increase the nanoplate coverage to 100% while keeping the layer thickness small. Moreover, we have also adjusted the thickness of TPBi in the perovskite nanoplate LEDs, and the 35 nm thick TPBi layer discussed above achieved the best device EQE value due to the balanced charge carriers in the emitting layer (see Figure S4 in the Supporting Information for more details). For future work, different charge transport layers could be explored to further optimize charge balance to increase the efficiency.

CONCLUSIONS

In summary, we demonstrated a color-pure 410 nm violet-light-emitting diode using layered perovskite $(\text{PEA})_2\text{PbBr}_4$ as the luminescent material. This violet LED based on solution-processed perovskite materials is made possible by using a 2D layered perovskite instead of the more common 3D perovskites. These functional room-temperature LEDs are based on a 2D perovskite active material with a reasonable efficiency. Furthermore, a DMF vapor annealing step was found to be crucial in enhancing the overall semiconductor and photo-physical properties of $(\text{PEA})_2\text{PbBr}_4$ perovskites and enable the fabrication of room-temperature-operable devices by converting polycrystalline $(\text{PEA})_2\text{PbBr}_4$ thin films to micrometer-sized nanoplates that yielded high-quality diodes with low subthreshold leakage currents and significantly enhanced EQE. This solvent vapor annealing method can be generally employed to increase the crystal grain size of perovskite materials and

improve their semiconductor properties and hence enhance the performance of various optoelectronic devices including solar cells, LEDs, and photodetectors. Further studies will focus on improving the surface coverage of the nanoplates on various substrates to further enhance optoelectronic device metrics and further investigating other charge transport layers to improve charge balance within the perovskite LEDs.

METHODS

Synthesis of 2-Phenylethylammonium (or Phenethylammonium) Bromide ($C_6H_5CH_2CH_2NH_3Br$). The 2-phenylethylammonium bromide was synthesized by a similar method reported previously. Briefly, a solution of HBr (48 wt % in water) was added slowly to 2-phenylethylamine with an equal molar ratio in a flask at 0 °C. Then the water was evaporated at an elevated temperature until the 2-phenethylammonium bromide crystals precipitated from the solution. After the solution was cooled, the powder product was filtered and rinsed with diethyl ether several times before it was dried at 80 °C in a vacuum oven for ~24 h to remove the residual water.

Preparation of Layered Perovskite $(PEA)_2PbBr_4$ Thin Films. The poly(3,4-ethylenedioxythiophene):poly(styrenesulfonate) (PEDOT:PSS)-coated indium tin oxide (ITO) glass substrates were prepared by spin-coating PEDOT:PSS (Baytron P VP Al 4083) onto an ITO substrate at 4000 rpm for 1 min and annealing at 140 °C for 30 min in a nitrogen-filled glovebox. The ITO (150 nm thick) on glass (1/2 in. × 1/2" in.) substrates was purchased from Thin Film Devices. The PEDOT:PSS solution was filtered through a 0.45 μ m nylon filter before use. The perovskite precursor solution was prepared by mixing PEA₂Br and PbBr₂ (Sigma-Aldrich) in a molar ratio of 2:1 in anhydrous *N,N*-dimethylformamide, forming a solution with a concentration of 6.7 wt %. The solution was spin-coated at 3000 rpm for 30 s on a PEDOT:PSS-coated ITO substrate and annealed at 100 °C for 10 min, creating a greenish thin film on the substrate.

Preparation of Layered Perovskite $(PEA)_2PbBr_4$ Nanoplates by Solvent Vapor Annealing. First, the $(PEA)_2PbBr_4$ perovskite was spin-coated on a 0.5 × 0.5 in. PEDOT:PSS-coated ITO substrate to form a layer of thin film with a speed of 3000 rpm for 30 s. Then the substrate was placed face-down on the edge of a cover glass, which was later placed in a beaker containing DMF, as illustrated in Figure 2D. The DMF liquid level was well below the cover glass, so that the substrate was protected from being immersed into DMF. The beaker containing the cover glass and substrate was covered by a larger cover glass in order to create a closed space for DMF vapor. After the beaker was held by hand, the DMF was heated with body temperature to about 30 °C. After a couple of minutes, a thin layer of DMF liquid droplets was observed to condense on the underside of the larger cover glass. A small amount of DMF vapor was able to diffuse beneath the upside-down substrate and come into contact with the spin-coated perovskite thin film thanks to the curvature of the cover glass. As soon as the color of the perovskite sample changed from greenish to purple due to the changed light scattering of nanoplates, the substrate was quickly removed from the closed system. Typically, this solvent vapor annealing process should be done in 3 to 5 min. If part of perovskite thin film was not converted into nanoplates upon examination under an optical microscope, the substrate should be put back into the closed system and treated again for a few more minutes until all the perovskite thin film was converted into nanoplates on the substrate. Last, the substrate was baked at 100 °C for 10 min in air. The thickness of the nanoplate layer created by this DMF solvent vapor annealing treatment was found to depend on the concentration of the precursor solution and the spin-coating speed.

Structural and Optical Characterizations. The SEM images were collected on a LEO SUPRA 55 VP field-emission scanning electron microscope operated at 3 kV. The AFM images were taken using an Agilent 5500 AFM. The PXRD data were collected using a Bruker D8 Advance powder X-ray diffractometer with Cu $K\alpha$ radiation. PL lifetimes were measured with $(PEA)_2PbBr_4$ thin-film or nanoplate samples deposited on plain glass substrates using a HORIBA FL 3-22 time-correlated single-photon-counting instrument

with a pulsed LED (HORIBA NanoLED, pulse duration: 1.4 ns) as light source operating at 371 nm. Steady-state PL spectra were measured by the same spectrofluorometer with 370 nm excitation from a Xe arc lamp. Fluorescence quantum yields of layered perovskite $(PEA)_2PbBr_4$ thin film and nanoplates were determined relative to 10 wt % of 9,10-diphenylanthracene in a poly(methyl methacrylate) host.⁴⁶

Device Fabrication and Characterization. After perovskite thin film or nanoplate preparation on PEDOT:PSS-coated ITO substrates, the samples were transferred into a vacuum deposition chamber where layers of 2,2',2''-(1,3,5-benzinetriyl)-tris(1-phenyl-1*H*-benzimidazole) (TPBi), calcium (Ca), and aluminum (Al) were sequentially deposited by thermal evaporation in a ultrahigh vacuum (<10⁻⁶ Torr). Ca and Al were deposited with a metal shadow mask to define the top electrodes. The current density–voltage (*J*–*V*) dependence was measured using a Keithley 6487 picoammeter/voltage source. Simultaneously, the light emission from the device was monitored by the photodiode current using a Newport 818 UV photodiode connected to a Newport 1835-C multifunction optical meter. Then the photodiode current and device current were converted into the number of photons and electrons, respectively, for external quantum efficiency calculation. EL spectrum was measured using a Horiba Scientific Fluorolog-3 spectrofluorometer, while the device was powered by a Keithley 2400 voltage source.

Ultraviolet Photoemission Spectroscopy Measurement of $(PEA)_2PbBr_4$. UPS measurements were performed on both the $(PEA)_2PbBr_4$ thin-film and nanoplate samples deposited on hydrogen-flame-annealed gold films in a home-built UHV multichamber system (PHI Electronics Inc., Eden Prairie, MN, USA) with base pressure better than 1 × 10⁻⁹ Torr. The UPS source was from a helium discharge lamp ($h\nu = 21.22$ eV). The photoelectrons are measured by a model 10-360 hemispherical analyzer. Samples were measured at a 0° electron takeoff angle, and the Fermi level was determined using a platinum reference sample. For all spectra the Fermi level was shifted to zero.

ASSOCIATED CONTENT

Supporting Information

The Supporting Information is available free of charge on the ACS Publications website at DOI: 10.1021/acsnano.6b02683.

UPS data of the $(PEA)_2PbBr_4$ thin-film and nanoplate samples, additional optical images of the sample morphology, the dependence of LED device performance on the precursor solution concentration and TPBi layer thicknesses (PDF)

AUTHOR INFORMATION

Corresponding Authors

*E-mail (T. L. Andrew): tlandrew@wisc.edu.

*E-mail (S. Jin): jin@chem.wisc.edu.

Author Contributions

§D. Liang and Y. Peng contributed equally to this work.

Notes

The authors declare no competing financial interest.

ACKNOWLEDGMENTS

D.L., Y.F., M.J.S., J. Zhai, Y.Z., R.J.H., and S.J. acknowledge financial support from the Department of Energy, Office of Basic Energy Sciences, Division of Materials Sciences and Engineering, under Award DE-FG02-09ER46664. Y.P., J. Zhang, and T.L.A. gratefully acknowledge financial support from the Air Force Office of Scientific Research, Grant FA9550-14-1-0128. M.J.S. also thanks the NSF Graduate Research Fellowship for support.

REFERENCES

- (1) Pust, P.; Schmidt, P. J.; Schnick, W. A Revolution in Lighting. *Nat. Mater.* **2015**, *14*, 454–458.
- (2) Reineke, S. Complementary LED Technologies. *Nat. Mater.* **2015**, *14*, 459–462.
- (3) Lee, J.; Chen, H.-F.; Batagoda, T.; Coburn, C.; Djurovich, P. I.; Thompson, M. E.; Forrest, S. R. Deep Blue Phosphorescent Organic Light-Emitting Diodes with Very High Brightness and Efficiency. *Nat. Mater.* **2016**, *15*, 92–98.
- (4) Koike, M.; Shibata, N.; Kato, H.; Takahashi, Y. Development of High Efficiency GaN-Based Multiquantum-Well Light-Emitting Diodes and Their Applications. *IEEE J. Sel. Top. Quantum Electron.* **2002**, *8*, 271–277.
- (5) Joseph, S.; Ruth, S. Organic Light-Emitting Devices (OLEDs) and OLED-Based Chemical and Biological Sensors: An Overview. *J. Phys. D: Appl. Phys.* **2008**, *41*, 133001.
- (6) Xiao, D.; Zhao, S.; Yuan, H.; Yang, X. CE Detector Based on Light-Emitting Diodes. *Electrophoresis* **2007**, *28*, 233–242.
- (7) Nakamura, S.; Senoh, M.; Mukai, T. High-Power InGaN/GaN Double-Heterostructure Violet Light Emitting Diodes. *Appl. Phys. Lett.* **1993**, *62*, 2390–2392.
- (8) Kojima, A.; Teshima, K.; Shirai, Y.; Miyasaka, T. Organometal Halide Perovskites as Visible-Light Sensitizers for Photovoltaic Cells. *J. Am. Chem. Soc.* **2009**, *131*, 6050–6051.
- (9) Lee, M. M.; Teuscher, J.; Miyasaka, T.; Murakami, T. N.; Snaith, H. J. Efficient Hybrid Solar Cells Based on Meso-Superstructured Organometal Halide Perovskites. *Science* **2012**, *338*, 643–647.
- (10) Liu, M.; Johnston, M. B.; Snaith, H. J. Efficient Planar Heterojunction Perovskite Solar Cells by Vapour Deposition. *Nature* **2013**, *501*, 395–398.
- (11) Zhou, H.; Chen, Q.; Li, G.; Luo, S.; Song, T.-b.; Duan, H.-S.; Hong, Z.; You, J.; Liu, Y.; Yang, Y. Interface Engineering of Highly Efficient Perovskite Solar Cells. *Science* **2014**, *345*, 542–546.
- (12) Stranks, S. D.; Eperon, G. E.; Grancini, G.; Menelaou, C.; Alcocer, M. J. P.; Leijtens, T.; Herz, L. M.; Petrozza, A.; Snaith, H. J. Electron-Hole Diffusion Lengths Exceeding 1 Micrometer in an Organometal Trihalide Perovskite Absorber. *Science* **2013**, *342*, 341–344.
- (13) Xing, G.; Mathews, N.; Sun, S.; Lim, S. S.; Lam, Y. M.; Grätzel, M.; Mhaisalkar, S.; Sum, T. C. Long-Range Balanced Electron- and Hole-Transport Lengths in Organic-Inorganic $\text{CH}_3\text{NH}_3\text{PbI}_3$. *Science* **2013**, *342*, 344–347.
- (14) Dong, Q.; Fang, Y.; Shao, Y.; Mulligan, P.; Qiu, J.; Cao, L.; Huang, J. Electron-Hole Diffusion Lengths > 175 μm in Solution-Grown $\text{CH}_3\text{NH}_3\text{PbI}_3$ Single Crystals. *Science* **2015**, *347*, 967–970.
- (15) Deschler, F.; Price, M.; Pathak, S.; Klüntberg, L. E.; Jarausch, D.-D.; Hügler, R.; Hüttner, S.; Leijtens, T.; Stranks, S. D.; Snaith, H. J.; Ataç, M.; Phillips, R. T.; Friend, R. H. High Photoluminescence Efficiency and Optically Pumped Lasing in Solution-Processed Mixed Halide Perovskite Semiconductors. *J. Phys. Chem. Lett.* **2014**, *5*, 1421–1426.
- (16) Yang, B.; Dyck, O.; Poplawsky, J.; Keum, J.; Puzos, A.; Das, S.; Ivanov, I.; Rouleau, C.; Duscher, G.; Geohegan, D.; Xiao, K. Perovskite Solar Cells with Near 100% Internal Quantum Efficiency Based on Large Single Crystalline Grains and Vertical Bulk Heterojunctions. *J. Am. Chem. Soc.* **2015**, *137*, 9210–9213.
- (17) Tan, Z.-K.; Moghaddam, R. S.; Lai, M. L.; Docampo, P.; Hügler, R.; Deschler, F.; Price, M.; Sadhanala, A.; Pazos, L. M.; Credgington, D.; Hanusch, F.; Bein, T.; Snaith, H. J.; Friend, R. H. Bright Light-Emitting Diodes Based on Organometal Halide Perovskite. *Nat. Nanotechnol.* **2014**, *9*, 687–692.
- (18) Cho, H.; Jeong, S.-H.; Park, M.-H.; Kim, Y.-H.; Wolf, C.; Lee, C.-L.; Heo, J. H.; Sadhanala, A.; Myoung, N.; Yoo, S.; Im, S. H.; Friend, R. H.; Lee, T.-W. Overcoming the Electroluminescence Efficiency Limitations of Perovskite Light-Emitting Diodes. *Science* **2015**, *350*, 1222–1225.
- (19) Yakunin, S.; Sytnyk, M.; Krieger, D.; Shrestha, S.; Richter, M.; Matt, G. J.; Azimi, H.; Brabec, C. J.; Stangl, J.; Kovalenko, M. V.; Heiss, W. Detection of X-Ray Photons by Solution-Processed Lead Halide Perovskites. *Nat. Photonics* **2015**, *9*, 444–449.
- (20) Wong, A. B.; Lai, M.; Eaton, S. W.; Yu, Y.; Lin, E.; Dou, L.; Fu, A.; Yang, P. Growth and Anion Exchange Conversion of $\text{CH}_3\text{NH}_3\text{PbX}_3$ Nanorod Arrays for Light-Emitting Diodes. *Nano Lett.* **2015**, *15*, 5519–5524.
- (21) Fang, Y.; Dong, Q.; Shao, Y.; Yuan, Y.; Huang, J. Highly Narrowband Perovskite Single-Crystal Photodetectors Enabled by Surface-Charge Recombination. *Nat. Photonics* **2015**, *9*, 679–686.
- (22) Stranks, S. D.; Snaith, H. J. Metal-Halide Perovskites for Photovoltaic and Light-Emitting Devices. *Nat. Nanotechnol.* **2015**, *10*, 391–402.
- (23) Xing, G.; Mathews, N.; Lim, S. S.; Yantara, N.; Liu, X.; Sabba, D.; Grätzel, M.; Mhaisalkar, S.; Sum, T. C. Low-Temperature Solution-Processed Wavelength-Tunable Perovskites for Lasing. *Nat. Mater.* **2014**, *13*, 476–480.
- (24) Zhu, H.; Fu, Y.; Meng, F.; Wu, X.; Gong, Z.; Ding, Q.; Gustafsson, M. V.; Trinh, M. T.; Jin, S.; Zhu, X. Y. Lead Halide Perovskite Nanowire Lasers with Low Lasing Thresholds and High Quality Factors. *Nat. Mater.* **2015**, *14*, 636–642.
- (25) Kim, Y.-H.; Cho, H.; Heo, J. H.; Kim, T.-S.; Myoung, N.; Lee, C.-L.; Im, S. H.; Lee, T.-W. Multicolored Organic/Inorganic Hybrid Perovskite Light-Emitting Diodes. *Adv. Mater.* **2015**, *27*, 1248–1254.
- (26) Wang, J.; Wang, N.; Jin, Y.; Si, J.; Tan, Z.-K.; Du, H.; Cheng, L.; Dai, X.; Bai, S.; He, H.; Ye, Z.; Lai, M. L.; Friend, R. H.; Huang, W. Interfacial Control Toward Efficient and Low-Voltage Perovskite Light-Emitting Diodes. *Adv. Mater.* **2015**, *27*, 2311–2316.
- (27) Song, J.; Li, J.; Li, X.; Xu, L.; Dong, Y.; Zeng, H. Quantum Dot Light-Emitting Diodes Based on Inorganic Perovskite Cesium Lead Halides (CsPbX_3). *Adv. Mater.* **2015**, *27*, 7162–7167.
- (28) Zhang, X.; Lin, H.; Huang, H.; Reckmeier, C.; Zhang, Y.; Choy, W. C. H.; Rogach, A. L. Enhancing the Brightness of Cesium Lead Halide Perovskite Nanocrystal Based Green Light-Emitting Devices through the Interface Engineering with Perfluorinated Ionomer. *Nano Lett.* **2016**, *16*, 1415–1420.
- (29) Li, G.; Rivarola, F. W. R.; Davis, N. J. L. K.; Bai, S.; Jellicoe, T. C.; de la Peña, F.; Hou, S.; Ducati, C.; Gao, F.; Friend, R. H.; Greenham, N. C.; Tan, Z.-K. Highly Efficient Perovskite Nanocrystal Light-Emitting Diodes Enabled by a Universal Crosslinking Method. *Adv. Mater.* **2016**, *28*, 3528.
- (30) Sadhanala, A.; Ahmad, S.; Zhao, B.; Giesbrecht, N.; Pearce, P. M.; Deschler, F.; Hoyer, R. L. Z.; Gödel, K. C.; Bein, T.; Docampo, P.; Dutton, S. E.; De Volder, M. F. L.; Friend, R. H. Blue-Green Color Tunable Solution Processable Organolead Chloride–Bromide Mixed Halide Perovskites for Optoelectronic Applications. *Nano Lett.* **2015**, *15*, 6095–6101.
- (31) Cheng, Z.; Lin, J. Layered Organic–Inorganic Hybrid Perovskites: Structure, Optical Properties, Film Preparation, Patterning and Templating Engineering. *CrystEngComm* **2010**, *12*, 2646–2662.
- (32) Mitzi, D. B. Templating and Structural Engineering in Organic–Inorganic Perovskites. *J. Chem. Soc., Dalton Trans.* **2001**, 1–12.
- (33) Saparov, B.; Mitzi, D. B. Organic–Inorganic Perovskites: Structural Versatility for Functional Materials Design. *Chem. Rev.* **2016**, *116*, 4558–4596.
- (34) Kitazawa, N.; Watanabe, Y. Optical Properties of Natural Quantum-Well Compounds ($\text{C}_6\text{H}_5\text{-C}_n\text{H}_{2n}\text{-NH}_3$) $_2\text{PbBr}_4$ ($n = 1\text{--}4$). *J. Phys. Chem. Solids* **2010**, *71*, 797–802.
- (35) Dou, L.; Wong, A. B.; Yu, Y.; Lai, M.; Kornienko, N.; Eaton, S. W.; Fu, A.; Bischak, C. G.; Ma, J.; Ding, T.; Ginsberg, N. S.; Wang, L.-W.; Alivisatos, A. P.; Yang, P. Atomically Thin Two-Dimensional Organic-Inorganic Hybrid Perovskites. *Science* **2015**, *349*, 1518–1521.
- (36) Kawano, N.; Koshimizu, M.; Sun, Y.; Yahaba, N.; Fujimoto, Y.; Yanagida, T.; Asai, K. Effects of Organic Moieties on Luminescence Properties of Organic–Inorganic Layered Perovskite-Type Compounds. *J. Phys. Chem. C* **2014**, *118*, 9101–9106.
- (37) Takagi, H.; Kunugita, H.; Ema, K. Influence of the Image Charge Effect on Excitonic Energy Structure in Organic-Inorganic

Multiple Quantum Well Crystals. *Phys. Rev. B: Condens. Matter Mater. Phys.* **2013**, *87*, 125421.

(38) Kitazawa, N. Excitons in Two-Dimensional Layered Perovskite Compounds: $(\text{C}_6\text{H}_5\text{C}_2\text{H}_4\text{NH}_3)_2\text{Pb}(\text{Br},\text{I})_4$ and $(\text{C}_6\text{H}_5\text{C}_2\text{H}_4\text{NH}_3)_2\text{Pb}(\text{Cl},\text{Br})_4$. *Mater. Sci. Eng., B* **1997**, *49*, 233–238.

(39) Saba, M.; Quochi, F.; Mura, A.; Bongiovanni, G. Excited State Properties of Hybrid Perovskites. *Acc. Chem. Res.* **2016**, *49*, 166–173.

(40) Era, M.; Morimoto, S.; Tsutsui, T.; Saito, S. Organic-Inorganic Heterostructure Electroluminescent Device Using a Layered Perovskite Semiconductor $(\text{C}_6\text{H}_5\text{C}_2\text{H}_4\text{NH}_3)_2\text{PbI}_4$. *Appl. Phys. Lett.* **1994**, *65*, 676–678.

(41) Chondroudis, K.; Mitzi, D. B. Electroluminescence from an Organic–Inorganic Perovskite Incorporating a Quaterthiophene Dye within Lead Halide Perovskite Layers. *Chem. Mater.* **1999**, *11*, 3028–3030.

(42) Jeon, N. J.; Noh, J. H.; Kim, Y. C.; Yang, W. S.; Ryu, S.; Seok, S. I. Solvent Engineering for High-Performance Inorganic–Organic Hybrid Perovskite Solar Cells. *Nat. Mater.* **2014**, *13*, 897–903.

(43) Bi, C.; Wang, Q.; Shao, Y.; Yuan, Y.; Xiao, Z.; Huang, J. Non-Wetting Surface-Driven High-Aspect-Ratio Crystalline Grain Growth for Efficient Hybrid Perovskite Solar Cells. *Nat. Commun.* **2015**, *6*, 7747.

(44) Xiao, Z.; Dong, Q.; Bi, C.; Shao, Y.; Yuan, Y.; Huang, J. Solvent Annealing of Perovskite-Induced Crystal Growth for Photovoltaic-Device Efficiency Enhancement. *Adv. Mater.* **2014**, *26*, 6503–6509.

(45) Shi, D.; Adinolfi, V.; Comin, R.; Yuan, M.; Alarousu, E.; Buin, A.; Chen, Y.; Hoogland, S.; Rothenberger, A.; Katsiev, K.; Losovyj, Y.; Zhang, X.; Dowben, P. A.; Mohammed, O. F.; Sargent, E. H.; Bakr, O. M. Low Trap-State Density and Long Carrier Diffusion in Organolead Trihalide Perovskite Single Crystals. *Science* **2015**, *347*, 519–522.

(46) Fu, Y.; Meng, F.; Rowley, M. B.; Thompson, B. J.; Shearer, M. J.; Ma, D.; Hamers, R. J.; Wright, J. C.; Jin, S. Solution Growth of Single Crystal Methylammonium Lead Halide Perovskite Nanostructures for Optoelectronic and Photovoltaic Applications. *J. Am. Chem. Soc.* **2015**, *137*, 5810–5818.

(47) Brown, T. M.; Kim, J. S.; Friend, R. H.; Cacialli, F.; Daik, R.; Feast, W. J. Built-in Field Electroabsorption Spectroscopy of Polymer Light-Emitting Diodes Incorporating a Doped Poly(3,4-ethylene dioxythiophene) Hole Injection Layer. *Appl. Phys. Lett.* **1999**, *75*, 1679–1681.

(48) D'Andrade, B. W.; Holmes, R. J.; Forrest, S. R. Efficient Organic Electrophosphorescent White-Light-Emitting Device with a Triple Doped Emissive Layer. *Adv. Mater.* **2004**, *16*, 624–628.

(49) Park, Y.; Choong, V.; Ettetdgui, E.; Gao, Y.; Hsieh, B. R.; Wehrmeister, T.; Müllen, K. Energy Level Bending and Alignment at the Interface between Ca and a Phenylene Vinylene Oligomer. *Appl. Phys. Lett.* **1996**, *69*, 1080–1082.

(50) Kahn, A. Fermi Level, Work Function and Vacuum Level. *Mater. Horiz.* **2016**, *3*, 7–10.

(51) Steckel, J. S.; Zimmer, J. P.; Coe-Sullivan, S.; Stott, N. E.; Bulović, V.; Bawendi, M. G. Blue Luminescence from $(\text{CdS})\text{ZnS}$ Core–Shell Nanocrystals. *Angew. Chem., Int. Ed.* **2004**, *43*, 2154–2158.

(52) Shirasaki, Y.; Supran, G. J.; Bawendi, M. G.; Bulovic, V. Emergence of Colloidal Quantum-Dot Light-Emitting Technologies. *Nat. Photonics* **2013**, *7*, 13–23.